JOURNAL OF PROPULSION AND POWER
Vol. 11, No. 2, March–April 1995

Navier–Stokes Analysis of Turbine Flowfield and External Heat Transfer

J. Luo* and B. Lakshminarayana†
Pennsylvania State University, University Park, Pennsylvania 16802

An explicit two-dimensional Navier–Stokes code has been modified and used to analyze the aerodynamics and heat transfer of a transonic turbine cascade. This code is based on a four-stage Runge–Kutta scheme. An algebraic Reynolds stress model (ARSM) and two versions of low Reynolds number two-equation turbulence models have been employed in the computation. Detailed comparisons are made between the predictions and the data measured by Arts et al. at the von Kármán Institute. An evaluation of the performance of different turbulence models for turbine aerodynamics and heat transfer has been carried out. The surface pressure distributions and wake profiles are predicted well by all the models. Reasonably good predictions have been obtained for the blade heat transfer by the k-ε and the k-ε/ARSM models. The k-ε/ARSM model appears to be able to capture, qualitatively, the anisotropy associated with bypass transition. A boundary-layer code was also used to predict heat transfer for comparison with the elliptic Navier–Stokes solutions.

Nomenclature

C = chord length
C_p = specific heat at constant pressure
C_μ, C_1, C_2, C_1', C_2', C_t = turbulence modeling parameters
d = diameter
e = internal energy per unit mass
f_μ, f_μ = near-wall damping functions
H = heat transfer coefficient, W/m²k
h = enthalpy per unit mass
K = acceleration factor
k = turbulent kinetic energy
L = turbulence length scale/ semiwake width
M = Mach number
n = normal distance to the surface
P = production rate of turbulent kinetic energy/stagnation pressure
P_{ij} = production rate of Reynolds stress
Pr_l, Pr_t = Prandtl numbers
p = pressure
q = turbulence velocity scale, $\sqrt{k}$
q_i = Cartesian components of heat transfer rate vector
Re = Reynolds number
S = coordinate along blade surface (positive for SS and negative for PS)
S' = distance from the center of trailing-edge circle in nominal exit flow direction
T = temperature
Tu_i = turbulence intensity components
t = time
U = magnitude of total velocity
u, v, w = Cartesian velocity components
u_τ = friction velocity
x = coordinate along axial chord
y = coordinate in tangential direction, pitchwise
y^+ = wall distance variable, (yu_τ/ν)
β = flow angle
γ = under-relaxation factor for solving ARSM equations
δ = boundary-layer thickness
δ_{ij} = Kronecker delta
ε = isotropic component of turbulent kinetic energy dissipation rate
ζ = loss coefficient
μ_l, μ_t = molecular, turbulent viscosity
ν = kinematic viscosity
ρ = density
τ_{ij} = Cartesian components of stress tensor
ϕ_{ij} = pressure-strain correlation
ω = specific dissipation rate of turbulent kinetic energy, ε/k

Subscripts

ax = axial
e = boundary-layer edge
i, j = streamwise, pitchwise
is = isentropic
LE, TE = leading edge, trailing edge
l, t = laminar, turbulent
PS = pressure surface
ref = reference
SS = suction surface
w = wall
0 = stagnation condition
1, 2 = cascade inlet, exit condition
∞ = inlet freestream

Superscripts

$''$ = fluctuating quantity in density averaging
$\sim$ = density-weighted time-averaged quantity
$-$ = time-averaged quantity

Presented as AIAA Paper 93-7075 at the 11th International Symposium on Air Breathing Engines, Tokyo, Japan, Sept. 1993; received Oct. 23, 1993; revision received July 14, 1994; accepted for publication July 15, 1994.

*Graduate Assistant, Center for Gas Turbine and Power. Student Member AIAA.

†Evan Pugh Professor of Aerospace Engineering, Director of Center for Gas Turbine and Power. Fellow AIAA.

Introduction

A THOROUGH knowledge and predictive capability of turbine aerodynamics and heat transfer is necessary to achieve higher turbine inlet temperatures and to minimize various losses, including profile loss, trailing-edge loss, and cooling loss. However, the turbine cascade flow and thermal fields are very complex due to the existence of many flow phenomena including laminar, transitional, and turbulent flows; stagnation flow; transonic flow; streamline curvature; high freestream turbulence; and unsteady vortex shedding at the trailing edge. Detailed measurements of the flow and thermal quantities, especially in rotating passages, are cumbersome, expensive, and in many cases, impossible. Computational fluid dynamics (CFD) techniques are very attractive for the investigation of these flows.

Inviscid codes are still commonly used in practice to predict turbine aerodynamics. Boundary-layer codes[1] have been developed to predict the profile loss and convective heat transfer on turbine blades. Predictions from parabolic boundary-layer codes are generally sensitive to the specifications of the initial profile and flow quantities at the edge of the boundary layer. In order to predict detailed flow and thermal characteristics, the Reynolds-averaged Navier–Stokes equations have to be solved.[2–4]

There has been an increased use of transport-equation turbulence models, such as the two-equation models (k-ε, k-ω, q-ω, etc.), especially their low Reynolds number versions, for the computation of viscous turbomachinery flows. The isotropic two-equation models still have some serious deficiencies as discussed in Lakshminarayana[5] and Speziale,[6] but they have yielded significantly improved predictions compared to those from zero-equation models for many complex flows. Boyle[7] computed heat transfer of seven turbine vane and blade geometries using an explicit quasi-three-dimensional thin-layer Navier–Stokes code with a modified Baldwin–Lomax model. Choi and Knight[8] calculated aerodynamics and heat transfer of a low aspect ratio turbine with an implicit three-dimensional thin-layer Navier–Stokes code and the q-ω model. There were some discrepencies between the predicted heat transfer rates and the measured values. Predictions of turbine blade heat transfer rates were also made by Ameri et al.[9] using a two-dimensional thin-layer Navier–Stokes code and the q-ω model. Dunn et al.[10] measured and computed the surface pressure and Stanton number distributions for a full two-stage turbine. The Stanton number distributions for the vane pressure surface were consistently underpredicted by all the computations.

Kunz and Lakshminarayana[11] developed an explicit two-dimensional Navier–Stokes code (hereafter referred to as RK2D) using the four-stage Runge–Kutta scheme. The Chien's[12] low Reynolds number k-ε model was used in their computation. The objective of the present work is to modify the RK2D by incorporating a new two-layer k-ε/ARSM model and the q-ω model,[13,14] to evaluate the performances of different models by computing the aerodynamics and heat transfer measured by Arts et al.[15] in a transonic turbine cascade. Chien's k-ε model and Coakley's q-ω model were chosen due to their good numerical stability. The purpose of utilizing the ARSM is to evaluate its capability in capturing the streamline curvature effects and the anisotropy of turbulence quantities in the turbine cascade flowfield. A two-dimensional boundary-layer code—TEXSTAN[16] was also employed to predict heat transfer for comparison with the Navier–Stokes solutions.

Theoretical Formulation

Mean-Flow Equations

The Favre (density-weighted time) averaging is used for both the mean flow and turbulence equations. The resulting two-dimensional continuity, momentum, and energy equations can be written in conservative form in Cartesian coordinates as

$$\frac{\partial \bar{\rho}}{\partial t} + \frac{\partial}{\partial x_j}(\bar{\rho}\tilde{u}_j) = 0 \tag{1}$$

$$\frac{\partial(\bar{\rho}\tilde{u}_i)}{\partial t} + \frac{\partial}{\partial x_j}(\bar{\rho}\tilde{u}_i\tilde{u}_j) = -\frac{\partial \bar{p}}{\partial x_i} + \frac{\partial}{\partial x_j}(\tau_{ij}) \tag{2}$$

$$\frac{\partial(\bar{\rho}\tilde{e}_0)}{\partial t} + \frac{\partial}{\partial x_j}(\bar{\rho}\tilde{u}_j\tilde{h}_0) = \frac{\partial}{\partial x_i}(\tilde{u}_j\tau_{ij} - q_i) \tag{3}$$

Two-Equation Turbulence Models

Using eddy-viscosity models, the effective stress tensor and the effective heat flux vector in the above mean-flow equations can be written in Cartesian coordinates as

$$\tau_{ij} = \tau_{lij} - \overline{\rho u_i'' u_j''} = (\mu_l + \mu_t)\left[\left(\frac{\partial \tilde{u}_i}{\partial x_j} + \frac{\partial \tilde{u}_j}{\partial x_i}\right) - \frac{2}{3}\delta_{ij}\frac{\partial \tilde{u}_k}{\partial x_k}\right] - \frac{2}{3}\delta_{ij}\bar{\rho}\tilde{k} \tag{4}$$

$$q_i = -C_p\frac{\mu_l}{Pr_l}\frac{\partial \tilde{T}}{\partial x_i} + \overline{\rho u_i'' h''} = -C_p\left(\frac{\mu_l}{Pr_l} + \frac{\mu_t}{Pr_t}\right)\frac{\partial \tilde{T}}{\partial x_i} \tag{5}$$

In the low Reynolds number k-ε model, the eddy viscosity in Eqs. (4) and (5) is obtained from the Prandtl–Komogorov relation:

$$\mu_t = C_\mu f_\mu \bar{\rho}\tilde{k}^2/\tilde{\varepsilon} \tag{6}$$

where k and ε are obtained by solving the transport equations for k and ε. Chien's k-ε model[12] is used in compressible form, and the detailed equations can be found in Kunz and Lakshminarayana.[11] For comparison purposes, the low Reynolds number q-ω model[14] (also in compressible form) is used in the following computations. In the q-ω model, q is defined as $q = \sqrt{k}$, and ω is defined as $\omega = \varepsilon/k$. The q-ω model[13,14] was essentially developed from the standard k-ε model and differed from Chien's model mainly in the near-wall damping functions.

Algebraic Reynolds Stress Model

Although the Reynolds stress models (RSM) have been shown to have significant advantage over eddy-viscosity models in capturing curvature, rotation, and three dimensionality,[5] their applications have been limited to simple flows due to the computational intensity of solving several "stiff" turbulence equations. By assuming that the convective and diffusive transport of individual Reynolds stress components are locally proportional to the transport of turbulent kinetic energy,[17] the differential equations in the RSM can be reduced to nonlinear algebraic equations, i.e., the algebraic Reynolds stress model (ARSM).

In the present investigation, a two-layer k-ε/ARSM model is adopted to capture the anisotropy of turbulence and curvature effects. The low Reynolds number k-ε model is used in the near-wall viscous sublayer and buffer layer, and the ARSM is used in the fully turbulent region (e.g., $y^+ > 50$). In the ARSM, the Reynolds stress components are defined as

$$-\overline{\rho u_i'' u_j''} = -\bar{\rho}\tilde{k}[(P_{ij} - 2P\delta_{ij}/3)(1 - C_2) + \phi_{ij,w}]/[P + \bar{\rho}\tilde{\varepsilon}(C_1 - 1)] - \tfrac{2}{3}\delta_{ij}\bar{\rho}\tilde{k} \tag{7}$$

where

$$P_{ij} = -\overline{\rho u_i'' u_k''}\partial\tilde{u}_j/\partial x_k - \overline{\rho u_j'' u_k''}\partial\tilde{u}_i/\partial x_k \quad \text{and} \quad P = P_{ii}/2 \tag{8}$$

and the near-wall term of $\phi_{ij,w}$ due to Gibson and Launder[18] is given by

$$\phi_{ij,w} = \phi_{ijw,1} + \phi_{ijw,2} \tag{9}$$

where

$$\phi_{ijw,1} = C_1'(\tilde{\varepsilon}/\tilde{k})(\overline{\rho u_k'' u_m''} n_k n_m \delta_{ij} - \tfrac{3}{2}\overline{\rho u_i'' u_k''} n_k n_j - \tfrac{3}{2}\overline{\rho u_j'' u_k''} n_k n_i) f_n \tag{10}$$

$$\phi_{ijw,2} = C_2'(\phi_{km,2} n_k n_m \delta_{ij} - \tfrac{3}{2}\phi_{ik,2} n_k n_j - \tfrac{3}{2}\phi_{jk,2} n_k n_i) f_n \tag{11}$$

In Eq. (11), $\phi_{ij,2} = -C_2(P_{ij} - \frac{2}{3}\delta_{ij}P)$ is the "rapid" part of pressure-strain correlation, and n_j is the unit vector normal to the surface. The damping function f_n is given by $f_n = \tilde{k}^{3/2}/(2.55\tilde{\varepsilon}n)$. The constants are $C_1 = 1.8$, $C_2 = 0.6$, $C_1' = 0.5$, and $C_2' = 0.3$. The k-ε model is matched with the ARSM at $y^+ = 50$. Since the low Reynolds number k-ε model is used in the near-wall region and its damping function f_μ implicitly accounts for the near-wall pressure strain correlation, the $\phi_{ij,w}$ may be dropped from Eq. (7). The matching of the k-ε model and the ARSM without $\phi_{ij,w}$ is taken at $y^+ = 200$, where f_μ is about 0.90, which is quite close to its fully turbulent value of 1.0.

The system of algebraic equations (for $-\overline{\rho u''u''}$, $-\overline{\rho v''v''}$ and $-\overline{\rho u''v''}$) is solved by direct matrix inversion. During the iteration, the two normal components are required to remain positive and to be less than twice the $\tilde{k}$. In order to further stabilize the solution procedure in early stages of iteration, the three components are also under-relaxed as

$$-\overline{\rho u_i'' u_j''} = (1 - \gamma)(-\overline{\rho u_i'' u_j''})_{\text{old}} + \gamma(-\overline{\rho u_i'' u_j''})_{\text{new}} \tag{12}$$

where $\gamma = 0.3$ is used. The convergent k-ε solutions are used to initialize the k-ε/ARSM computation.

In the two-equation models, a constant turbulent Prandtl number Pr_t is used to compute the turbulent heat flux. However, there are experimental evidences indicating that the heat transfer in turbulent flow is not driven by an isotropic eddy diffusivity.[19] Measurements in pipes and boundary layers show that the turbulent heat fluxes in the flow direction are two to three times larger than that normal to the surface, even though the streamwise temperature gradient is negligible compared to that normal to the surface. In the following computations with the ARSM, the General Gradient Diffusion Hypothesis (GGDH[19]), for turbulent heat flux is compared with the constant Prandtl number approach. Adopting the GGDH, the turbulent heat flux can be expressed as

$$\overline{\rho u_i'' h''} = -C_p C_t \frac{\tilde{k}}{\tilde{\varepsilon}} \overline{\rho u_i'' u_j''} \frac{\partial \tilde{T}}{\partial x_j} \tag{13}$$

where $C_t = 0.3$. Unlike the constant Prandtl number approach, this model accounts for the turbulent heat flux in the direction without temperature gradient.

Numerical Procedure

Navier-Stokes Code—RK2D

A standard four-stage Runge–Kutta scheme[20] is used by the RK2D.[11] The fourth-order artificial dissipation is included to damp high wave number errors, and the second-order artificial dissipation is used to improve the shock capturing, as suggested in Ref. 20. The second-order artificial dissipation is included in the two turbulence transport equations (of k and ε or q and ω) to enhance convergence, because the convection terms are also discretized with second-order accurate central differences. Anisotropic scaling of artificial dissipation terms due to Martinelli[21] was used. Multiplied by the square of the normalized local velocity $(U/U_\infty)^2$, the smoothing in both the momentum and turbulence equations was reduced to zero near the wall to avoid contamination of the solution by excessive dissipation. Local variable time-stepping was used to improve convergence.

On the Cray Y-MP at NASA Huntsville, the execution CPU s/(gridpoint*iteration) of the RK2D is 1.77×10^{-5} and 1.45×10^{-5}, using the two-layer k-ε/ARSM model and the k-ε model, respectively. The H-grid is employed in the RK2D. The use of a combination of algebraic and elliptic methods[22] makes it possible to generate a smooth grid while maintaining strict control over grid spacing and orthogonality near the wall boundary. The orthogonal grid near the wall is highly desirable for the implementation of low Reynolds number turbulence models.

For the von Kármán Institute (VKI) cascade computations, the inlet boundary is specified at the same location as that of the experiments, i.e., $x/C_{ax} = -1.487$ ($x = 0.0$ at the leading edge). To minimize nonuniformity of back pressure caused by the wake, the outlet boundary is extended beyond the experimental "exit plane" ($x/C_{ax} = 1.433$) to locate at $x/C_{ax} = 1.9$. The back pressure is specified at the outlet since the axial component of outlet velocity is subsonic for all the cases.

For the k-ε model, k and isotropic dissipation rate ε are set to zero at the wall. Constant values of k and ε are imposed at the inlet based on specified freestream turbulence intensity and length scale:

$$\tilde{k}_\infty = 1.5(Tu_\infty \tilde{U}_\infty)^2 \quad \text{and} \quad \tilde{\varepsilon}_\infty = \tilde{k}_\infty^{1.5}/L_\infty \tag{14}$$

The freestream length scale is set equal to 1.5 mm for the turbine cascade flow, which is equal to the radius of the freestream grid turbulence generating rods. At the exit boundary, values of k and ε are extrapolated along $j = \text{const}$ grid lines. For the q-ω model, all the boundary conditions are set in the same way as the k-ε model, except the wall condition for ω

$$\left.\frac{\partial \omega}{\partial n}\right|_w = 0 \tag{15}$$

Boundary-Layer Code—TEXSTAN

The TEXSTAN code[16] is an extension of the STAN5.[1] It contains seven different two-equation turbulence models. Since it is not the purpose of the present investigation to compare different turbulence models in this boundary-layer code, only Chien's model is used to compute some cases for comparison with the elliptic Navier-Stokes solutions.

Flat Plate Boundary Layer

The three turbulence models, i.e., k-ε, q-ω, and k-ε/ARSM, were validated by computing a flat plate boundary layer. A

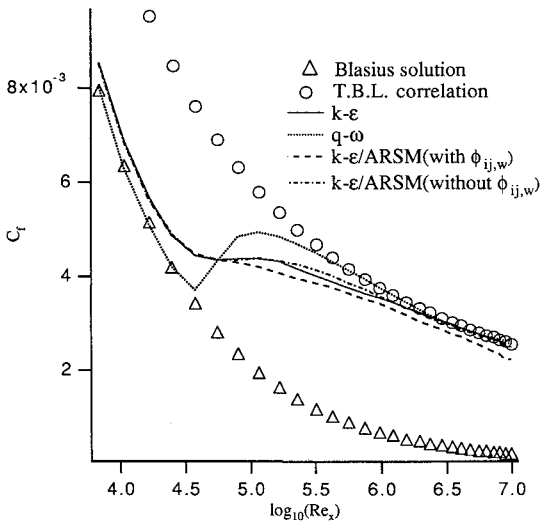

Fig. 1 Comparison of predicted skin friction coefficients for the flat-plate boundary layer.

33 × 33 grid was used for the computation. The grid and freestream conditions were chosen to provide a boundary-layer displacement thickness Reynolds number of 8000 near the exit of the computational domain to match Klebanoff's[23] experimental condition. The freestream Mach number was taken to be 0.5 to accommodate the compressible formulation of the RK2D. The inlet freestream turbulence intensity was specified as 3%.

The three models provided close predictions for near-wall mean velocity profile (u^+ vs y^+) and the turbulent shear stress profile. The predicted skin friction coefficients are shown in Fig. 1, where the turbulent boundary-layer correlation $C_f = 0.455/\ln^2(0.06Re_x)$ is from White.[24] The transition near the leading edge is predicted by all the models. The predicted distribution of turbulence intensities by the k-ε/ARSM without $\phi_{ij,w}$ is shown in Fig. 2, where $Tu_i = \sqrt{\overline{\rho u_i'' u_i''}/\bar{\rho}}/\tilde{U}_e$. The k-ε/ARSM without $\phi_{ij,w}$ is able to predict the difference between T_u and T_v, but it yields identical values for T_v and T_w.

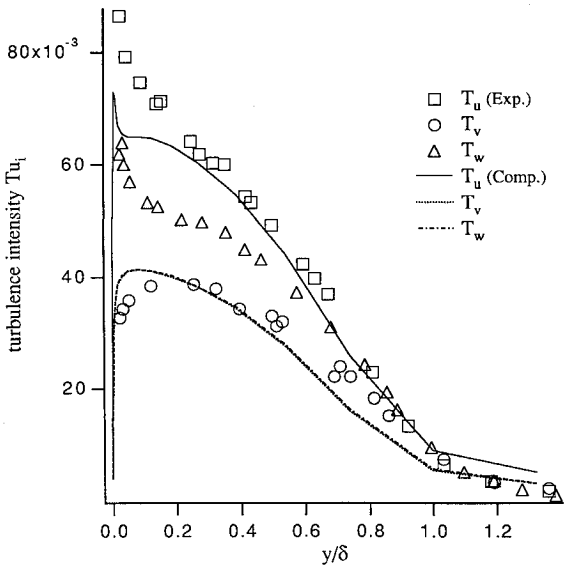

Fig. 2 Turbulence intensity profiles in the flat-plate turbulent boundary layer; experiment by Klebanoff; computation by the two-layer k-ε/ARSM without $\phi_{ij,w}$.

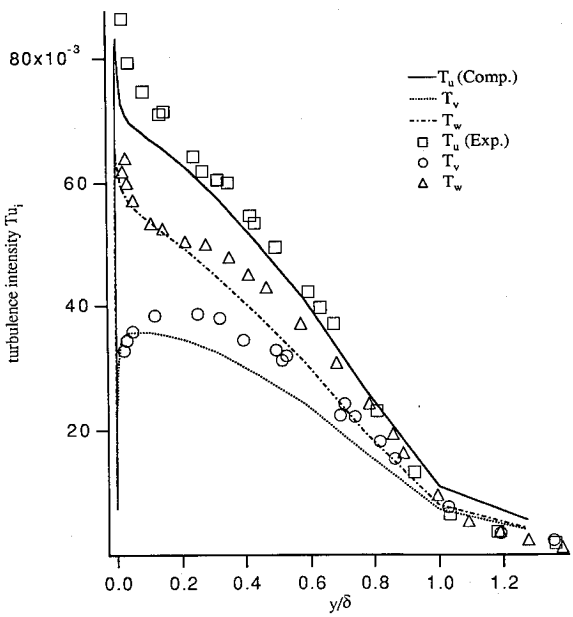

Fig. 3 Turbulence intensity profiles in the flat-plate turbulent boundary layer; experiment by Klebanoff; computation by the two-layer k-ε/ARSM with $\phi_{ij,w}$.

To distinguish T_v from T_w, the $\phi_{ij,w}$ has to be included in the ARSM. As seen in Fig. 3, the computed turbulence intensities by the k-ε/ARSM with $\phi_{ij,w}$ are in very good agreement with Klebanoff's data.[23] It should be noted that neither the k-ε model nor the q-ω model can capture any anisotropy of the turbulence.

Transonic Turbine Cascade

Although most two-equation models may yield close predictions for simple shear flows, their predictions for complex cascade flows may be quite different. One purpose of this article is to compare the performance of the three turbulence models for computing turbine flow and thermal quantities. The aerodynamics and blade heat transfer data of the VKI transonic linear turbine guide vane cascade measured by Arts et al.[15] was selected as the primary test case for the present work. This turbine blade shape was optimized for a downstream isentropic Mach number of 0.9. The downstream isentropic Reynolds number varied from 0.6 × 10^6 to 2.1 × 10^6. The total temperature at the inlet was around 410 K, and the blade wall temperature was constant at about 300 K for all the test runs. The freestream turbulence intensity varied from 1 to 6%. The inlet flow angle was $\beta_1 = 0$ (deg), $C = 67.65$ (mm), pitch/chord = 0.85, stagger angle = 55 (deg), $C_{ax} = 37.0$ (mm), and design outlet angle $\beta_2 = 74$ (deg). Table 1 shows all the cases computed in this article.

Initially, computations were carried out with a 139 × 91 mesh and a 129 × 71 mesh using the k-ε model. The predicted surface pressure and heat transfer using the 139 × 91 grid were found to be quite close to those obtained from the 129 × 71 grid. Considering the intensity of computing many cases with three different turbulence models, further refined grid was not tested and the 129 × 71 grid was used in the following computations. The grid clustering was adjusted for cases with different Reynolds numbers to ensure proper resolution of the near-wall viscous layer. The near-wall nodes are located at y^+ approximately equal to 1, and about 5–8 nodes are situated in the region $y^+ < 20$.

As stated above, the inclusion of $\phi_{ij,w}$ in the ARSM significantly improves the prediction of the turbulence quantities in the flat plate boundary layer. However, the k-ε/ARSM with $\phi_{ij,w}$ and the k-ε/ARSM without $\phi_{ij,w}$ yielded similar predictions for the VKI cascade flow. The reason may be due to the fact that both the ARSMs (with and without $\phi_{ij,w}$) are used beyond $y^+ = 200$, and thus, f_μ is close to zero in most areas except the near-wall region of the turbulent boundary layer. No convergent solution was obtained when the ARSM with $\phi_{ij,w}$ was used down to $y^+ = 50$. The problem may be with the matching of these two models as well as the awkward expression of $\phi_{ij,w}$ on highly curved turbine blades. In their airfoil flow computation with the same ARSM, Davidson and Rizzi[25] found that $\phi_{ij,w}$ gave too small damping of the shear stress in the separation region. They had to use a simplified form (which essentially assumed the airfoil surface to be a plane surface), to reach better agreement with the data.

For two-dimensional flows, the lateral component of Reynolds stress ($-\rho\overline{w''w''}$) does not appear in the mean flow equa-

Table 1 Description of test cases

Case/condition	P_{01}, bar	$Re_{is,2}$, 10^6	$M_{is,2}$	Tu_z, %
Mur043	1.435	1.0	0.840	1
Mur049	1.608	1.0	1.020	1
Mur129	1.849	1.14	0.840	1
Mur217	1.835	1.16	0.934	4
Mur222	0.822	0.55	1.135	6
Mur235	1.828	1.15	0.927	6
Mur239	3.387	2.14	0.922	6
Mur251	1.827	1.0	0.890	1
Mur264	0.910	0.5	0.970	1
Mur272	1.895	1.0	1.095	1

tions. The k-ε/ARSM model without $\phi_{ij,w}$ will be used in the following computations since it can also predict T_u and T_v quite well (see Fig. 2). The computations for each case, by three different models, were carried out with the identical grids, boundary conditions, artificial dissipation rates, and convergence criteria. Typically, three orders of magnitude drop of the rms density residual and two to two-and-a-half orders of magnitude drop of the rms turbulent kinetic energy (or q for the q-ω model) residual were taken as convergence criteria.

Flowfield Computation

The isentropic Mach number distribution for the transonic case Mur049 ($M_{is,2} = 1.02$, $Re_{is,2} = 1.0 \times 10^6$, and $Tu_\infty = 1\%$) is plotted in Fig. 4. The blade isentropic Mach number, including the effect of shock wave, is captured well by all the computations. The computed (by the k-ε model) and measured shock wave patterns (schlieren visualization) are shown in Fig. 5. The computed shock wave is presented as divergence of velocity contours. The location and strength of the shock wave is captured quite well. Figure 6 shows the comparison of computed and measured wake profiles at $x/C_{ax} = 1.433$. All the models' predictions are good, with the k-ε prediction being the best. The wake width and depth computed by the k-ε/ARSM appears to be larger than that computed by the k-ε model. Since the diffusive transport of turbulence is important in the wake, the k-ε/ARSM cannot be expected to be more accurate than the k-ε model due to the limitation of its basic assumption.[17]

Arts et al.[15] measured the wake at only one location ($x/C_{ax} = 1.433$). Since the predictions are good at this location, an attempt was made to assess the structure and decay of the wake downstream of the cascade. The wake profiles at different downstream locations are shown in Fig. 7. The decay is rapid and the wake width is an appreciable portion of the pitch at $x/C_{ax} = 1.80$. The variation of the semiwake width downstream of the cascade is shown in Fig. 8. The semiwake width is defined as the width of the profile at half the depth (50% of maximum defect in total pressure) of the wake. This width is normalized by the wake-width L_{ref} at $x/C_{ax} = 1.25$. The downstream distance S' is normalized by the blade trailing-edge diameter.

In Fig. 8, the experimental semiwake width shown was derived from the wake profiles measured in a transonic turbine cascade by Mee et al.[26] The computed semiwake width for the subsonic case Mur043 is also included. It can be seen that the scaling of the semiwake width growth (width $\sim\sqrt{S'}$), used for isolated airfoil wakes in incompressible flows[27] and for low-speed compressor cascade wakes,[28] gives a reasonable

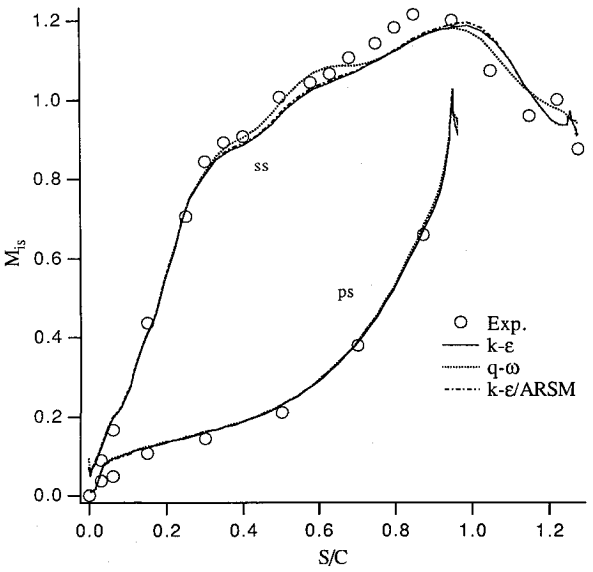

Fig. 4 Blade isentropic Mach number distribution for Mur049 ($M_{is,2} = 1.02$, $Re_{is,2} = 1.0 \times 10^6$, and $Tu_\infty = 1\%$).

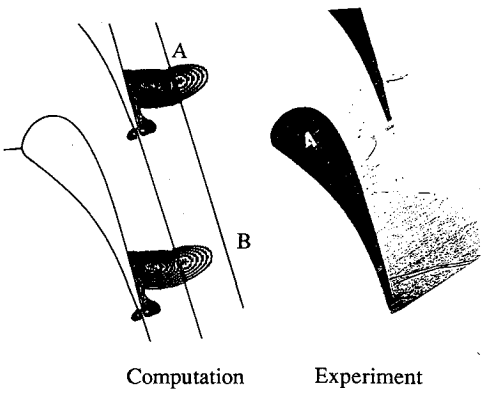

Fig. 5 Measured and computed shock wave pattern for Mur049, presented as divergence of velocity contours [−3500 to −9000 (s^{-1}) with contour interval being −500 (s^{-1})].

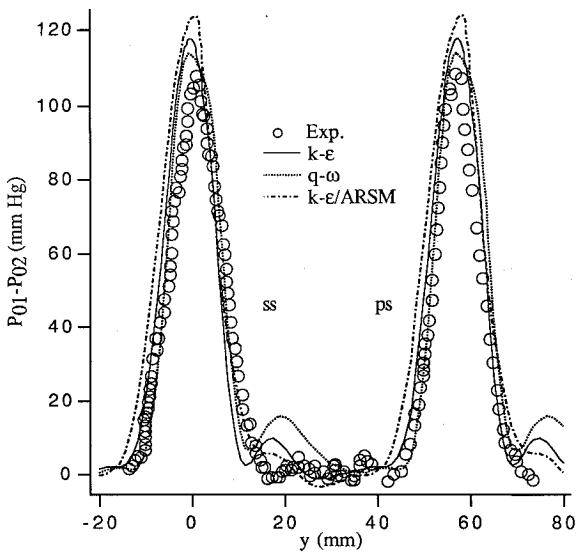

Fig. 6 Computed and measured wakes at $x/C_{ax} = 1.433$ for Mur049 ($M_{is,2} = 1.02$, $Re_{is,2} = 1.0 \times 10^6$, and $Tu_\infty = 1\%$).

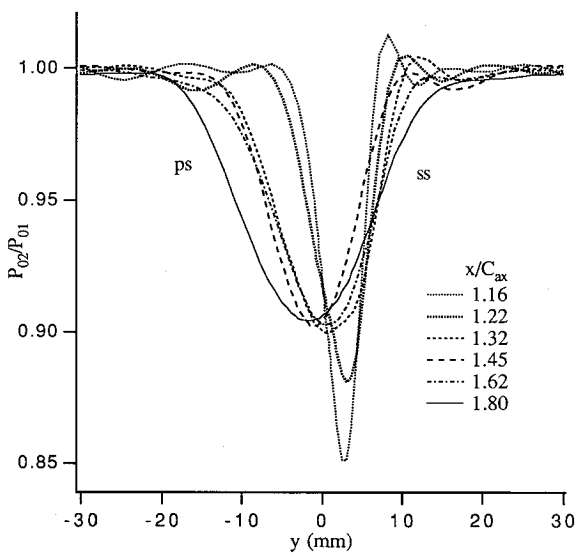

Fig. 7 Computed total pressure profiles (by the k-ε model) in the wake at different downstream locations for Mur049 ($M_{is,2} = 1.02$, $Re_{is,2} = 1.0 \times 10^6$, and $Tu_\infty = 1\%$).

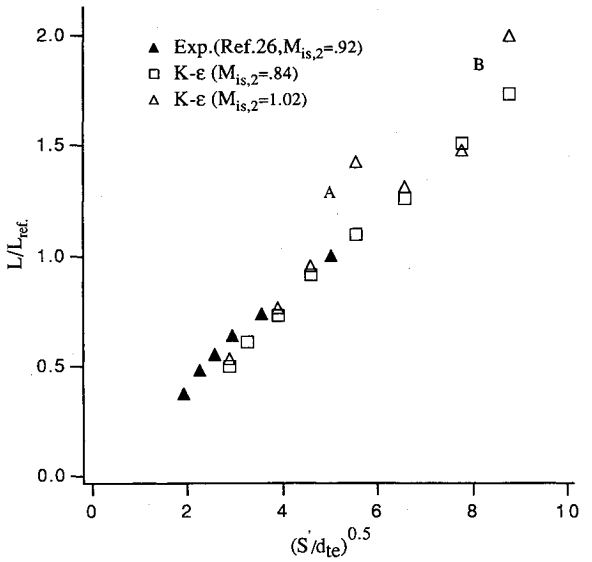

Fig. 8 Wake width growth downstream of the blade; S' = distance from the center of trailing-edge circle in nomimal exit flow direction, d_{te} = diameter of the trailing-edge circle.

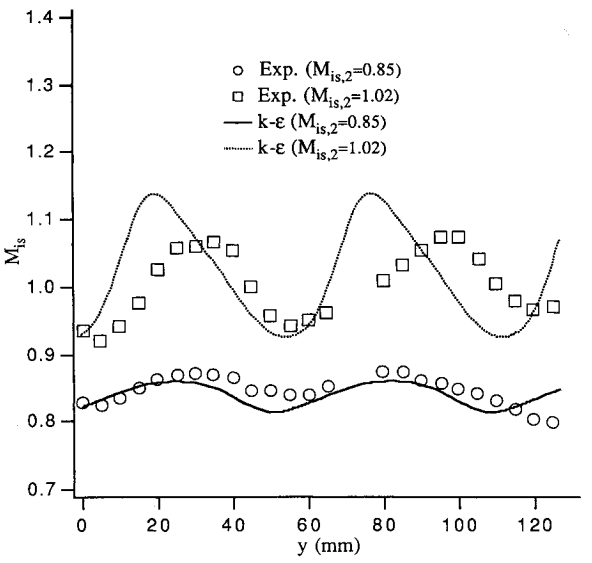

Fig. 9 Static pressure (expressed as M_{is}) variation at x/C_{ax} = 1.433 across two pitches ($Re_{is,2}$ = 1.0 × 10^6 and Tu_∞ = 1%).

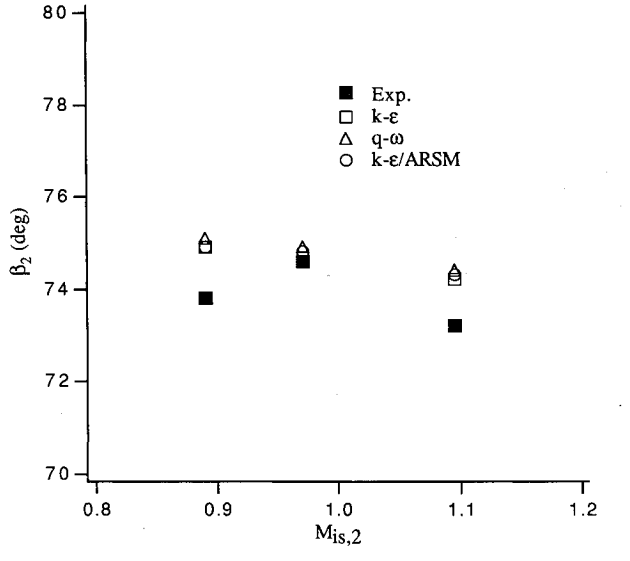

Fig. 10 Downstream flow angles for Mur251 ($M_{is,2}$ = 0.89, $Re_{is,2}$ = 1.0 × 10^6), Mur264 ($M_{is,2}$ = 0.97, $Re_{is,2}$ = 0.5 × 10^6), and Mur272 ($M_{is,2}$ = 1.095, $Re_{is,2}$ = 1.0 × 10^6), Tu_∞ = 1%.

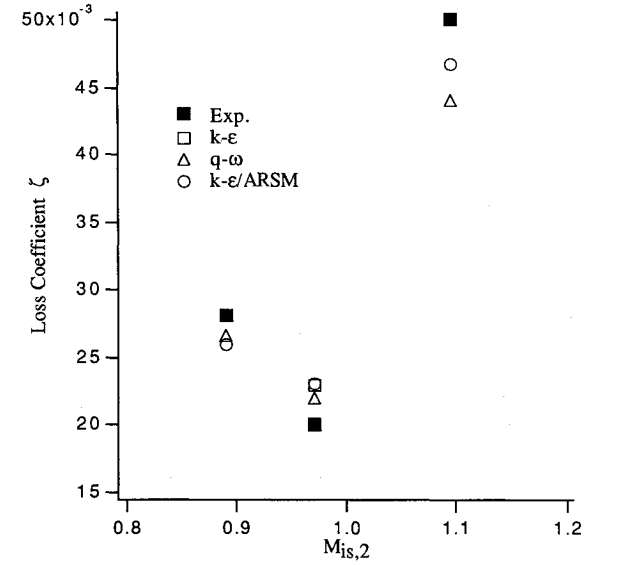

Fig. 11 Loss coefficients for cases in Fig. 10.

representation of the wake development for these two transonic turbine cascade wakes. The sudden increase in the wake width at downstream locations A and B (Fig. 8) is attributed to the shock/wake interaction. The locations of the suction side shock interacting with the wake is shown in Fig. 5. From Fig. 8, it is clear that the correlation is not valid when shock waves are present at the exit. Except for the shock/wake interaction region, the wake width follows the correlation.

To check for flow periodicity, Arts et al.[15] measured the static pressure distribution (expressed as isentropic Mach number distribution) across the passage. As stated earlier, the computational outlet boundary is extended beyond the experimental measurement station and located at x/C_{ax} = 1.90. The predicted variation of M_{is} across two pitches is compared with the measurements. For the subsonic outlet flow, the agreement is quite good, as shown in Fig. 9. For the supersonic outlet flow, the experimental profile is not completely periodic and the agreement is reasonably good. Both computations and data reveal significant variations of static and stagnation pressures across the wake for the transonic cascade.

The predicted and measured passage-averaged exit flow angles are shown in Fig. 10. All the computations predict the exit angles within the experimental accuracy. Since the wake profiles are predicted well by all the models, it is not surprising that the predicted passage-averaged loss coefficients are in agreement with the data, as shown in Fig. 11. The loss coefficient is defined as

$$\zeta = 1 - U_2^2/U_{is,2}^2$$
$$= 1 - [(p_2/P_{02})^{(\gamma-1)/\gamma}]/[1 - (p_2/P_{01})^{(\gamma-1)/\gamma}] \quad (16)$$

It should be noted that Tu_∞ = 1% for all the above cases. With such a low freestream turbulence level, the boundary layers on both surfaces are mostly laminar except near the rear of the suction surface. The major difference between Chien's and Coakley's models lies in the low-Reynolds number functions. However, in the fully turbulent wake, those low-Reynolds number functions are not effective, and essentially the high Reynolds number formulations are used. This may explain the close predictions from these two models.

Transition and Heat Transfer Prediction

The blade convective heat transfer strongly depends on the boundary-layer transition. It is known that the transition on the turbine blades is mainly influenced by the freestream turbulence and the streamwise pressure gradient. Increasing freestream turbulence promotes early transition, while large flow acceleration tends to delay transition. Influences also come from the Reynolds number and the Mach number, e.g., the shock wave location and its interaction with the boundary layer. Thus, to obtain accurate prediction of the transition and the heat transfer, the aerodynamic parameters must be captured accurately.

Figure 12 shows the acceleration factors along both surfaces for three typical cases (Mur222, Mur235, and Mur239). Defined as $K = (\nu/U_e^2)\, dU_e/dS$, the acceleration factor is a very important parameter for understanding turbine boundary-layer transition. For values of K larger than 3.0×10^{-6}, transition is suppressed for low Tu_∞, and the turbulent boundary layers begin to relaminarize. It should be noted that K depends not only on the pressure gradient but also on the Reynolds number. For the same surface pressure gradient, the higher the Reynolds number, the lower is the acceleration factor, and thus, the earlier the transition. As seen from Fig. 12, over almost the entire pressure surface, K is much larger than 3.0×10^{-6} for cases Mur222 and Mur235, and for this reason the boundary layer will probably remain laminar. On the suction surface, after initial large acceleration, the flow experiences a weak adverse pressure gradient for cases Mur235 and Mur239.

In Fig. 13, the predictions for the case Mur222 ($M_{is,2} = 1.14$, $Re_{is,2} = 0.55 \times 10^6$, and $Tu_\infty = 6\%$) by the k-ε model, the q-ω model, and the two-layer k-ε/ARSM model are shown. The flow is highly accelerated on both the surfaces and the transition is observed only near the trailing edge on the suction surface. The heat transfer rates on both the surfaces are predicted well by all the models except near the rear of the suction surface where the shock wave is located. The transition is triggered by the shock wave and has been captured by all the models. The boundary-layer code underpredicts the heat transfer on the pressure surface and the computation is terminated on the suction surface near the inception of separation.

For a higher Reynolds number, Mur 235 ($M_{is,2} = 0.93$, $Re_{is,2} = 1.15 \times 10^6$, and $Tu_\infty = 6\%$), the onset of transition is observed earlier along the suction side, which is captured by the k-ε and the k-ε/ARSM models (Fig. 14). The flow on the pressure surface is probably transitional, and the high freestream turbulence leads to the heat transfer increase, which has not been predicted well by the Navier-Stokes computations, however. The prediction using the GGDH formulation for turbulent heat flux is also plotted in Fig. 14. It can be seen that the GGDH prediction is quite close to that using the constant Pr_t. Boyle[7] reported that the effect of using variable Pr_t was rather small. The present result is consistent with Boyle's observation, supporting the use of constant Pr_t for computing the turbulent heat flux in thin boundary layers on turbine blades. The q-ω model does not capture transition for this case. However, Ameri and Arnone[29] found that the q-ω model predicted the location of transition better than the k-ε model. The reason may be partially due to the difference between version one that they used and version two[14] of the q-ω model used in this article.

To evaluate the ability of the k-ε/ARSM to predict the anisotropy of turbulence in turbine cascade flows, the normalized streamwise and normal components of Reynolds stress [$\rho u''u''/(2\rho k)$ and $\rho v''v''/(2\rho k)$] across the boundary layer at different streamwise locations are plotted in Fig. 15. Sharma et al.[30] have observed that most of the disturbance energy is contained in the streamwise component of turbulence inten-

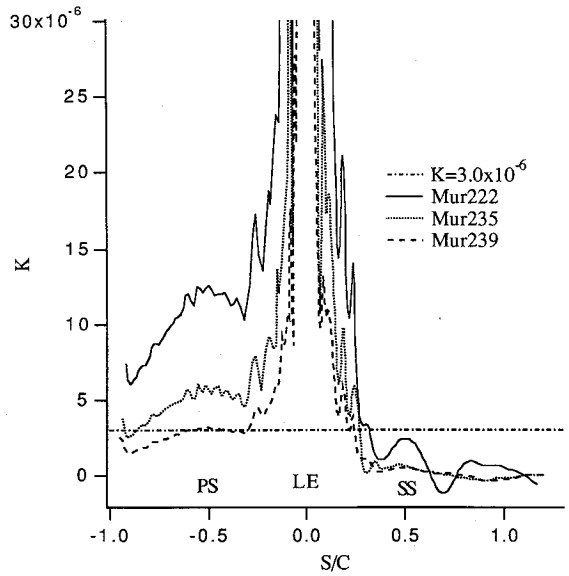

Fig. 12 Acceleration factors for Mur222, Mur235, and Mur239.

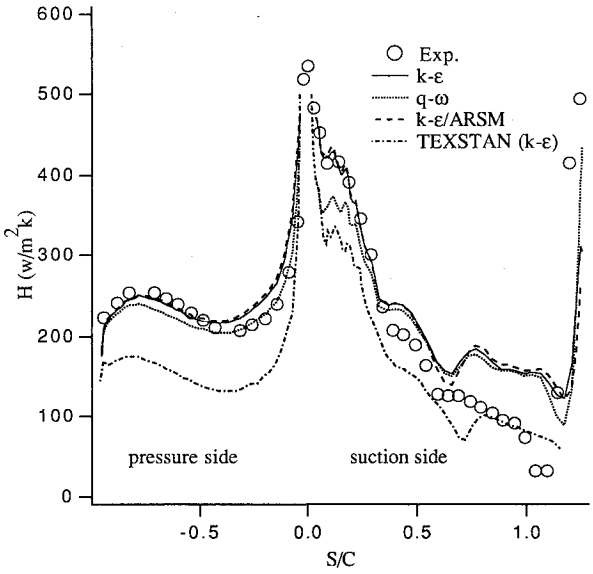

Fig. 13 Heat transfer prediction for Mur222 ($M_{is,2} = 1.14$, $Re_{is,2} = 0.55 \times 10^6$, and $Tu_\infty = 6\%$).

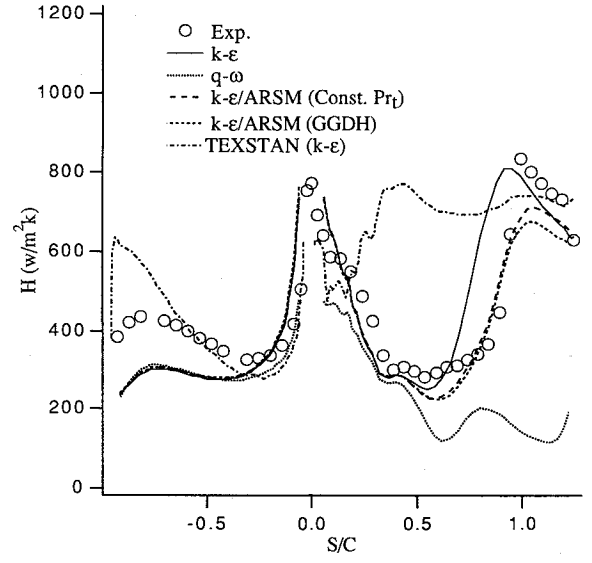

Fig. 14 Heat transfer prediction for Mur235 ($M_{is,2} = 0.93$, $Re_{is,2} = 1.15 \times 10^6$, and $Tu_\infty = 6\%$).

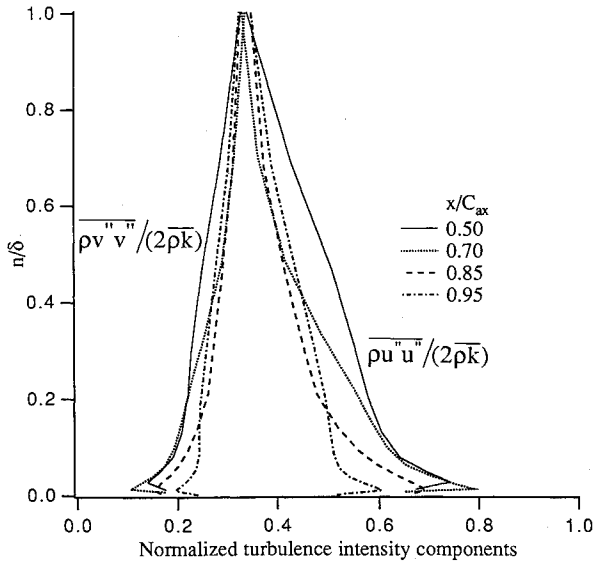

Fig. 15 Profiles of normalized turbulence intensity components (computed by k-ε/ARSM) at different axial chordwise locations on the suction surface for Mur235.

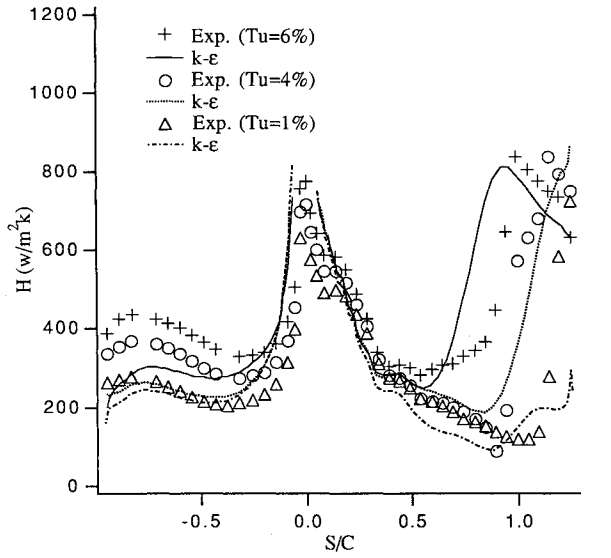

Fig. 16 Effect of freestream turbulence on blade heat transfer ($M_{is,2}$ = 0.93, $Re_{is,2}$ = 1.1 × 10^6, and Tu_∞ = 1, 4, and 6%).

sity before transition. During the transition, both the streamwise and normal components grow with the latter component growing at a faster rate than the former, resulting in a decrease of the relative magnitude of streamwise intensity. As can be seen from Fig. 15, this evolution of streamwise and normal turbulence intensity within the boundary layer during transition appears to be simulated qualitatively by the k-ε/ARSM model.

Figure 16 shows the influence of freestream turbulence levels ($M_{is,2}$ = 0.93, $Re_{is,2}$ = 1.1 × 10^6, and Tu_∞ = 1, 4, and 6%). Clearly, the freestream turbulence level has significant influence on the transition, which is captured by the k-ε model. Finally, Fig. 17 shows the predictions by the three turbulence models as well as the TEXSTAN for the case of highest Reynolds number and highest freestream turbulence level ($M_{is,2}$ = 0.92, $Re_{is,2}$ = 2.14 × 10^6 and Tu_∞ = 6%). Transition occurs on the suction surface at about S/C = 0.38, which is close to the end of flow acceleration (i.e., $S/C \approx 0.36$, see Fig. 12). The k-ε and the k-ε/ARSM models provide reasonably good predictions for the suction surface heat transfer. Despite the fact that the flow is highly accelerating over the pressure surface ($K > 3.0 \times 10^{-6}$ for about 50% distance, see Fig. 12), transition still occurs there. However, this transition was not captured by any model in the Navier–Stokes code. The k-ε/ARSM prediction is slightly better than that by the k-ε model. From Figs. 13, 14, and 17, it may be concluded that the high Reynolds number ARSM model does not have significant advantage over the two-equation model for the prediction of attached boundary layers on turbine nozzle blading. The rotor flow with large turning may need the ARSM.

It should be noted that the underprediction of pressure surface heat transfer has been reported by a number of researchers, e.g., Choi and Knight[8] and Dunn et al.[10] Sharma and Syed[31] argued that the higher than expected heat transfer on the pressure surface could be attributed to the high local turbulence levels and to large concave curvatures. A combination of these parameters may cause premature transition, which leads to much higher heat transfer due to increased turbulent mixing and by the formation of organized vortical flow structures (Taylor–Gortler vortices). However, the turbine pressure surface boundary layer is typically very thin, which results in a very low value of the curvature parameter δ/R (R = curvature radius, normally on the order of chord length), thus suggesting the insignificance of curvature effects.

Even though the parabolic boundary-layer code and the elliptic Navier–Stokes code use the same k-ε model, the former provides much better heat transfer prediction on the pressure side for this case (Fig. 17). This is partially due to the fact that the freestream turbulence level near the pressure surface predicted by the boundary-layer code (by solving an ordinary differential equation) is higher than that predicted by the Navier–Stokes code. As exhibited in Fig. 17 (and Fig. 14), Chien's k-ε model in the boundary-layer code predicts earlier transition on the suction surface, which was also observed by Harasgama et al.[32] for the same cascade flow. Indeed, Chien's model had been observed to predict a premature transition, e.g., in Ref. 33. In a recent review, Simoneau and Simon[34] made a similar comment. However, this model did provide reasonable predictions of heat transfer in the present Navier–Stokes computations, and similar performances were also observed by Hah[2] and Ameri and Arnone.[29] It should be noted that the elliptic Navier–Stokes method and the parabolic boundary-layer method have significant differences in the levels of numerical resolution and artificial dissipation, as well as the inflow conditions and freestream boundary conditions.

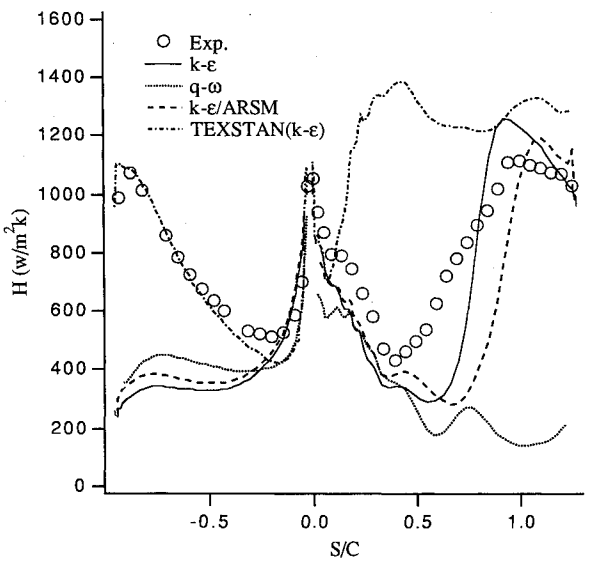

Fig. 17 Heat transfer prediction for Mur239 ($M_{is,2}$ = 0.93, $Re_{is,2}$ = 2.14 × 10^6, and Tu_∞ = 6%).

Concluding Remarks

An explicit two-dimensional Navier–Stokes code, with Chien's low Reynolds number k-ε model, Coakley's low

Reynolds number q-ω model, and a two-layer k-ε/ARSM model, was used to analyze the aerodynamics and heat transfer of a highly loaded transonic turbine cascade under various operating conditions. Blade surface pressure distributions, blade wakes, losses, and exit flow angles are captured well by all the three models. Only slight differences exist among predictions by different models. The computed shock wave location and strength are in good agreement with the measurements. The semiwake width increases with the square root of distance downstream of the blade. The correlation is not valid when shock waves are present near the cascade exit. Except for the shock/wake interaction region, the semiwake width follows the correlation developed for an isolated and cascade airfoil wakes.

Reasonably good predictions have been obtained for the blade external heat transfer rates for cases with different Reynolds numbers, Mach numbers, and freestream turbulence intensities. While the k-ε and the k-ε/ARSM models captured the onset of transition on the suction side, transition on the highly accelerating pressure side was not predicted well by the Navier–Stokes computation. In contrast, the parabolic boundary-layer code provided much better prediction than the elliptic Navier–Stokes code for the pressure surface transition and heat transfer. The two-layer k-ε/ARSM provides much improved predictions of turbulence quantities in boundary layers than isotropic two-equation models. The k-ε/ARSM model appears to be able to capture, qualitatively, the anisotropy associated with bypass transition. However, for the mean-flow parameters of the turbine boundary layer, no improved predictions have been obtained by the k-ε/ARSM model.

Further work may include the improvement of the low Reynolds number functions of the two-equation models and incorporation of intermittency concepts. To facilitate the application of Reynolds stress model in turbine flow computations, it is necessary to modify the formulations for the near-wall pressure-strain correlation $\phi_{ij,w}$.

Acknowledgments

This work was supported by NASA Contract NAS 8-38867 monitored by Lisa Griffin of Marshall Space Flight Center, Huntsville, Alabama. The assistance of R. Kunz, S. Fan, and J. Schwab is gratefully appreciated. The authors wish to acknowledge NASA for providing the supercomputing resources at NASA Lewis and Ames Research Centers.

References

[1]Crawford, M., and Kays, W., "STAN5—A Program for Numerical Computation of Two Dimensional Internal and External Boundary Layer Flows," NACA CR 2742, Dec. 1976.

[2]Hah, C., "Numerical Study of Three-Dimensional Flow and Heat Transfer near the Endwall of a Turbine Blade Row," AIAA Paper 89-1689, June 1989.

[3]Chima, R. V., "Inviscid and Viscous Flows in Cascades with an Explicit Multi-Grid Scheme," *AIAA Journal*, Vol. 23, No. 10, 1985, pp. 1556–1563.

[4]Rai, M. M., "Navier-Stokes Simulation of Rotor/Stator Interaction Using Patched and Overlaid Grids," *Journal of Propulsion and Power*, Vol. 3, No. 5, 1987, pp. 387–396.

[5]Lakshminarayana, B., "Turbulence Modelling for Complex Shear Flows," *AIAA Journal*, Vol. 24, No. 12, 1986, pp. 1900–1917.

[6]Speziale, C. G., "Discussion of Turbulence Modelling: Past and Future," Inst. for Computer Applications in Science and Engineering Rept. 89-58, July 1989.

[7]Boyle, R., "Navier-Stokes Analysis of Turbine Blade Heat Transfer," *Journal of Turbomachinery*, Vol. 113, No. 2, 1991, pp. 392–403.

[8]Choi, D., and Knight, C. J., "Aerodynamic and Heat Transfer Analysis for a Low Aspect Ratio Turbine Using a 3D Navier-Stokes Code," AIAA Paper 91-2240, June 1991.

[9]Ameri, A. A., Sockol, P. M., and Gorla, R. S. R., "Navier-Stokes Analysis of Turbomachinery Blade External Heat Transfer," *Journal of Propulsion and Power*, Vol. 8, No. 2, 1992, pp. 374–381.

[10]Dunn, M. G., Kim, J., Civinskas, K. C., and Boyle, R. J., "Time-Averaged Heat Transfer and Pressure Measurements and Comparisons with Prediction for a Two-Stage Turbine," American Society of Mechanical Engineers Paper 92-GT-194, Cologne, Germany, 1992.

[11]Kunz, R., and Lakshminarayana, B., "Explicit Navier-Stokes Computation of Cascade Flows Using the k-ε Model," *AIAA Journal*, Vol. 30, No. 1, 1992, pp. 13–22.

[12]Chien, K. Y., "Prediction of Channel and Boundary-Layer Flows with a Low-Reynolds Number Turbulence Model," *AIAA Journal*, Vol. 20, No. 1, 1982, pp. 33–38.

[13]Coakley, T. J., "Turbulence Modeling Methods for the Compressible Navier-Stokes Equations," AIAA Paper 83-1693, July 1983.

[14]Coakley, T. J., and Hsieh, T., "A Comparison Between Implicit and Hybrid Methods for the Calculation of Steady and Unsteady Inlet Flows," AIAA Paper 85-1125, July 1985.

[15]Arts, T., Rouvroit, M. L., and Rutherford, A. W., "Aero-Thermo Investigation of a Highly Loaded Transonic Linear Turbine Guide Vane Cascade," von Kármán Inst. TN 174, Sept. 1990; also, *Journal of Turbomachinery*, Vol. 114, No. 1, 1992, pp. 147–154.

[16]Crawford, M., and Stephens, C., "TEXSTAN Primer," Mechanical Engineering Dept., Univ. of Texas, Austin, TX, 1988.

[17]Rodi, W., "A New Algebraic Relation for Calculating Reynolds Stress," *ZAMM*, Vol. 56, 1976, pp. 219–221.

[18]Gibson, M., and Launder, B., "Ground Effects on Pressure Fluctuations in the Atmospheric Boundary Layer," *Journal of Fluid Mechanics*, Vol. 86, Pt. 3, 1978, pp. 491–511.

[19]Launder, B. E., "On the Computation of Convective Heat Transfer in Complex Turbulent Flows," *Journal of Heat Transfer*, Vol. 110, Nov. 1988, pp. 1112–1128.

[20]Jameson, A., Schmidt, W., and Turkel, E., "Numerical Solutions of Euler Equations by Finite Volume Methods Using Runge-Kutta Time-Stepping Schemes," AIAA Paper 81-1259, June 1981.

[21]Martinelli, L., "Calculation of Viscous Flows with Multigrid Methods," Ph.D. Dissertation, Mechanical and Aerospace Engineering Dept., Princeton Univ., Princeton, NJ, 1987.

[22]Basson, A. H., Kunz, R. F., and Lakshminarayana, B., "Grid Generation for Three-Dimensional Turbomachinery Geometries Including Tip Clearance," *Journal of Propulsion and Power*, Vol. 9, No. 1, 1993, p. 59.

[23]Klebanoff, P., "Characteristics of Turbulence in a Boundary Layer with Zero Pressure Gradient," NACA TN-3178, 1954.

[24]White, F. M., *Viscous Fluid Flow*, 2nd ed., McGraw–Hill, New York, 1991, p. 432.

[25]Davidson, L., and Rizzi, A., "Navier-Stokes Computation of Airfoil in Stall Using Algebraic Reynolds-Stress Model," AIAA Paper 92-0195, Jan. 1992.

[26]Mee, D. J., Baines, N. C., Oldfield, M. L. G., and Dickens, T. E., "An Examination of Contributions to the Loss on a Transonic Turbine Blade in Cascade," *Journal of Turbomachinery*, Vol. 114, Jan. 1992, pp. 155–162.

[27]Schlichting, H., *Boundary Layer Theory*, 7th ed., McGraw–Hill, New York, 1979.

[28]Raj, R., and Lakshminarayana, B., "Characteristics of the Wake Behind a Cascade of Airfoils," *Journal of Fluid Mechanics*, Vol. 61, Pt. 4, 1973, pp. 707–730.

[29]Ameri, A. A., and Arnone, A., "Navier-Stokes Turbine Heat Transfer Predictions Using Two-Equation Turbulence Closures," AIAA Paper 92-3067, July 1992.

[30]Sharma, O., Wells, R. A., Schlinker, R. H., and Bailey, D. A., "Boundary Layer Development on Turbine Airfoil Suction Surfaces," *Journal of Engineering for Power*, Vol. 104, July 1982, pp. 698–706.

[31]Sharma, O., and Syed, S., "Turbulence Modeling in Gas Turbine Design and Analysis," AIAA Paper 91-0514, Jan. 1991.

[32]Harasgama, S. P., Tarada, F. H., Baumann, R., Crawford, M. E., and Neelakantan, S., "Calculation of Heat Transfer to Turbine Blading Using Two-Dimensional Boundary Layer Methods," American Society of Mechanical Engineers Paper 93-GT-79, June 1993.

[33]Stephens, C., and Crawford, M., "An Investigation into the Numerical Prediction of Boundary Layer Transition Using the K. Y. Chien Turbulence Model," NASA CR-185252, 1990.

[34]Simoneau, R. J., and Simon, F. F., "Progress Towards Understanding and Predicting Heat Transfer in the Turbine Gas Path," *International Journal of Heat and Fluid Flow*, Vol. 14, No. 2, 1993, pp. 106–128.